ACTA IMEKO
ISSN: 2221-870X
December 2023, Volume 12, Number 4, 1 - 8

Using digital methods in active power measurement

Francisco Alegria[1]

[1] *Instituto de Telecomunicações and Instituto Superior Técnico/Universidade de Lisboa, Av. Rovisco Pais 1, 1049-001 Lisbon,Portugal*

ABSTRACT
Digitized voltage and current waveforms can be used to estimate active power by processing the obtained samples through two methods: Discrete Integration and Spectral Analysis. The former involves computing the average of the sample-by-sample product of the two waveforms, while the latter uses sine fitting algorithms to estimate the amplitude and initial phase of each waveform. Precision expressions for both estimators are derived as a function of the number of samples acquired and the amount of additive random noise present, which is useful for determining the confidence interval for measurements. The two estimators are compared, and it is concluded that the second method, using sine fitting, is sometimes superior.

Section: RESEARCH PAPER

Keywords: active power; measurement; digital; spectrum; sine fitting

Citation: Francisco Alegria, Using digital methods in active power measurement, Acta IMEKO, vol. 12, no. 4, article 45, December 2023, identifier: IMEKO-ACTA-12 (2023)-04-45

Section Editor: Laura Fabbiano, Politecnico di Bari, Italy

Received June 19, 2023; **In final form** December 12, 2023; **Published** December 2023

Funding: This work was supported by Instituto de Telecomunicações, Lisbon, Portugal.

Corresponding author: Francisco Alegria, e-mail: francisco.alegria@tecnico.ulisboa.pt

1. INTRODUCTION

In modern times, measurement devices have integrated microprocessors to augment their functionalities and adaptability. Typically, this entails an initial analog front end for signal conditioning, succeeded by an analog-to-digital converter (ADC) responsible for converting the relevant quantities into digital format [1], [2]. A microprocessor or microcontroller is then employed for digital signal processing and various other tasks. The solutions presented here have been the subject of a previous publication in the proceedings of a conference [3].

There are several methods commonly used to measure active power using digital methods where voltage and current waveforms are digitized:

Instantaneous Power Method: In this method, the instantaneous power is calculated as the product of the instantaneous voltage and current values at each sample point. The power samples are then averaged over a period to obtain the average active power.

Discrete Fourier Transform (DFT) Method: The DFT can be used to convert the digitized voltage and current waveforms from the time domain to the frequency domain. By multiplying the corresponding voltage and current frequency components, the active power can be calculated as the sum of the products.

Windowed-Sinc Filter Method: This method involves applying a windowed-sinc filter to the digitized voltage and current waveforms to obtain the filtered versions. The filtered waveforms are then multiplied point-wise, and the resulting waveform is integrated over time to obtain the active power.

Goertzel Algorithm: The Goertzel algorithm is a digital signal processing technique that can be used to calculate the power in a specific frequency component. By applying the Goertzel algorithm to the digitized voltage and current waveforms at the fundamental frequency, the active power can be measured.

Quadrature Component Method: This method involves calculating the quadrature (imaginary) components of the voltage and current waveforms by using digital signal processing techniques, such as Hilbert transform or complex least squares. The product of the quadrature components represents the reactive power and subtracting it from the instantaneous power yields the active power.

Extended Kalman Filter Method: The extended Kalman filter is a recursive estimation algorithm used to estimate the state of a system. By modelling the voltage and current waveforms as a state-space system and applying the extended Kalman filter, the active power can be estimated.

These methods vary in complexity and performance, and the choice of method depends on factors such as accuracy requirements, computational resources, and the specific characteristics of the current and voltage signals being measured.

2. MEASUREMENT SYSTEM

A similar methodology is applied in power and energy measurement. Voltage and current transducers are employed, yielding an output voltage or current that traverses a known resistor, resulting in a voltage that is subsequently converted into digital form, as illustrated in Figure 1. This traditional circuit configuration finds application in multiple systems discussed in existing literature [4]-[6].

The conventional method for calculating active power is the Discrete Integration Method. This method entails capturing a defined number of samples (M) from the voltage and current waveforms over an integer number of cycles and subsequently multiplying these samples together to obtain the instantaneous power ($v_n\ i_n$) on a per-sample basis. The resultant vector is then subjected to averaging in order to obtain the active power:

$$\hat{P} = \frac{1}{M}\sum_{n=1}^{M} v_n\, i_n. \tag{1}$$

If we presume the absence of any offset error requiring correction, a condition attainable by subtracting the product of the average voltage and current as outlined in [7], an alternative approach for active power estimation becomes viable. This method is gaining prominence, driven by the robust computational capabilities of contemporary microcontrollers and microprocessors. It revolves around a spectral analysis of the voltage and current waveforms, affording greater versatility by enabling the assessment of supplementary parameters like distortion and power quality metrics [8]-[9].

Spectral analysis can be conducted using either the three-parameter sine fitting (SF) or the Discrete Fourier Transform (DFT) approach [10]. In both of these techniques, the amplitude ($\hat{A}$) and initial phase ($\hat{\varphi}$) of every harmonic component within both the voltage and current are determined, as depicted in Figure 2.

When there are no harmonics present, the active power can be estimated with:

$$\hat{P} = \frac{1}{2}\,\widehat{A_{\mathrm{V}}}\,\widehat{A_{\mathrm{I}}}\cos(\widehat{\varphi_{\mathrm{V}}} - \widehat{\varphi_{\mathrm{I}}})\,. \tag{2}$$

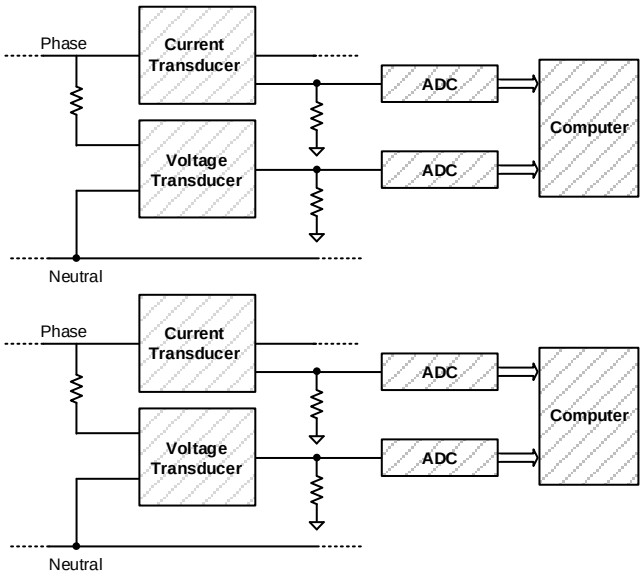

Figure 1. Block diagram of a power/energy measuring instrument.

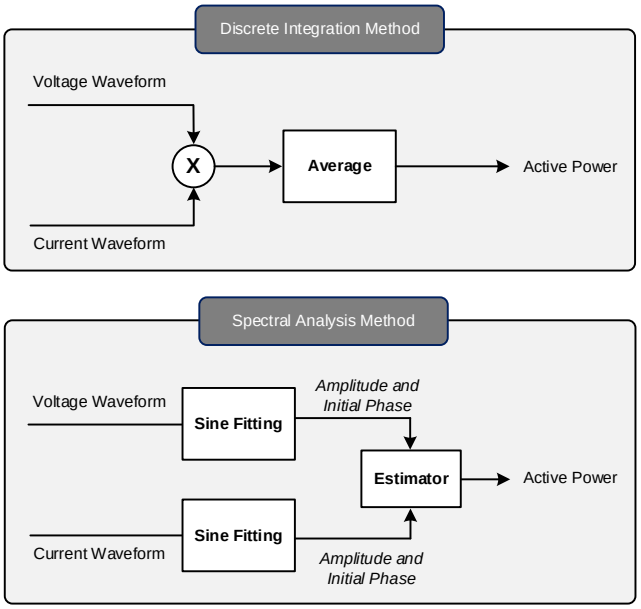

Figure 2. Illustration of the Discrete Integration Method and the Spectral Analysis Method of estimating active power.

The precision of the active power estimation can be influenced by several non-ideal factors, including random noise, sampling irregularities, frequency discrepancies, and quantization errors. This research specifically delves into the influence of random additive noise on the certainty of these estimations. It establishes mathematical expressions for computing the standard deviation of active power estimation for each of the two methods, considering factors like the number of collected samples and the standard deviation of additive noise in each data acquisition channel, as discussed in sections 2 and 3. These analytical formulations are subsequently utilized to determine the method that outperforms the other under identical measurement conditions, as elucidated in section 4. Finally, the last section presents conclusions regarding the performance of both methods and the utility of the derived analytical expressions.

3. SPECTRAL ANALYSIS METHOD

The two voltages at the input of both ADCs are given by

$$\begin{aligned} v_{\mathrm{ADC}_1}(t) &= V\,K_{\mathrm{V}}\cos(\omega\,t + \varphi_{\mathrm{V}}) + n_{\mathrm{ADC}_1}(t) \\ v_{\mathrm{ADC}_2}(t) &= I\,K_{\mathrm{I}}\cos(\omega\,t + \varphi_{\mathrm{I}}) + n_{\mathrm{ADC}_2}(t)\,. \end{aligned} \tag{3}$$

In this section, we will distinguish between two ADCs: ADC_1, which is responsible for digitizing the voltage-proportional waveform, and ADC_2, tasked with digitizing the current-proportional waveform. It's important to emphasize that both signals fed into these ADCs are in voltage form. The constants K_{V} and K_{I} relate the measured voltage and current to the ADC input voltage, respectively. These constants vary depending on the transducer in use and, if applicable, the sampling resistors, as illustrated in Figure 1. The variables n_{ADC_1} and n_{ADC_2} represent the random noise present at the ADC inputs. This noise may originate from the voltage and current being measured, the sensors, the signal conditioning circuit, or even the ADCs themselves [11]. Regardless of its source, this additive type of noise can be considered as present at the ADC input. It's also worth noting that the quantization error of the ADC can contribute to this noise.

With M data samples acquired from each channel a sine-fitting procedure is used to estimate the amplitudes, A_V and A_I, where

$$A_\mathrm{V} = V\,K_\mathrm{V} \;\text{ and }\; A_\mathrm{I} = I\,K_\mathrm{I}\,, \tag{4}$$

and initial phase (φ_V and φ_I). To estimate the power, one uses

$$\hat{P} = \frac{1}{2}\frac{\widehat{A_\mathrm{V}}\,\widehat{A_\mathrm{I}}}{K_\mathrm{V}\,K_\mathrm{I}}\cos(\widehat{\varphi_\mathrm{V}} - \widehat{\varphi_\mathrm{I}})\,. \tag{5}$$

The estimator standard deviation can be computed from the second moment with

$$E\{\hat{P}^2\} = E\left\{\left[\frac{1}{2}\frac{\widehat{A_\mathrm{V}}\,\widehat{A_\mathrm{I}}}{K_\mathrm{V}\,K_\mathrm{I}}\cos(\widehat{\varphi_\mathrm{V}} - \widehat{\varphi_\mathrm{I}})\right]^2\right\}. \tag{6}$$

After some manipulation one has

$$E\{\hat{P}^2\} = E\left\{\begin{array}{l}\frac{1}{4}\frac{\widehat{A_\mathrm{V}}^2}{K_\mathrm{V}^2}\cos^2(\widehat{\varphi_\mathrm{V}})\frac{\widehat{A_\mathrm{I}}^2}{K_\mathrm{I}^2}\cos^2(\widehat{\varphi_\mathrm{I}}) + \\ \frac{1}{4}\frac{\widehat{A_\mathrm{V}}^2}{K_\mathrm{V}^2}\sin^2(\widehat{\varphi_\mathrm{V}})\frac{\widehat{A_\mathrm{I}}^2}{K_\mathrm{I}^2}\sin^2(\widehat{\varphi_\mathrm{I}}) + \\ \frac{1}{2}\frac{\widehat{A_\mathrm{V}}}{K_\mathrm{V}}\cos(\widehat{\varphi_\mathrm{V}})\frac{\widehat{A_\mathrm{I}}}{K_\mathrm{I}}\cos(\widehat{\varphi_\mathrm{I}}) \times \\ \frac{\widehat{A_\mathrm{V}}}{K_\mathrm{V}}\sin(\widehat{\varphi_\mathrm{V}})\frac{\widehat{A_\mathrm{I}}}{K_\mathrm{I}}\sin(\widehat{\varphi_\mathrm{I}})\end{array}\right\}. \tag{7}$$

Using the properties of the expected value leads to

$$\begin{aligned}E\{\hat{P}^2\} = {} & \frac{1}{4\,K_\mathrm{V}^2\,K_\mathrm{I}^2}E\left\{\widehat{A_\mathrm{V}}^2\cos^2(\widehat{\varphi_\mathrm{V}})\right\}E\left\{\widehat{A_\mathrm{I}}^2\cos^2(\widehat{\varphi_\mathrm{I}})\right\} \\ & + \frac{1}{4\,K_\mathrm{V}^2\,K_\mathrm{I}^2}E\left\{\widehat{A_\mathrm{V}}^2\sin^2(\widehat{\varphi_\mathrm{V}})\right\}E\left\{\widehat{A_\mathrm{I}}^2\sin^2(\widehat{\varphi_\mathrm{I}})\right\} \\ & + \frac{1}{2\,K_\mathrm{V}^2\,K_\mathrm{I}^2}E\left\{\widehat{A_\mathrm{V}}^2\cos(\widehat{\varphi_\mathrm{V}})\sin(\widehat{\varphi_\mathrm{V}})\right\} \\ & \times E\left\{\widehat{A_\mathrm{I}}^2\cos(\widehat{\varphi_\mathrm{I}})\sin(\widehat{\varphi_\mathrm{I}})\right\}.\end{aligned} \tag{8}$$

Now, using (38), (39) and (40), given in the appendix, we can write (8) as

$$\begin{aligned}&E\{\hat{P}^2\} \\ &= \frac{\left(A_\mathrm{V}^2\cos^2(\varphi_\mathrm{V}) + \frac{2}{M}\sigma_\mathrm{V}^2\right)\times\left(A_\mathrm{I}^2\cos^2(\varphi_\mathrm{I}) + \frac{2}{M}\sigma_\mathrm{I}^2\right)}{4\,K_\mathrm{V}^2\,K_\mathrm{I}^2} \\ &+ \frac{\left(A_\mathrm{V}^2\sin^2(\varphi_\mathrm{V}) + \frac{2}{M}\sigma_\mathrm{V}^2\right)\times\left(A_\mathrm{I}^2\sin^2(\varphi_\mathrm{I}) + \frac{2}{M}\sigma_\mathrm{I}^2\right)}{4\,K_\mathrm{V}^2\,K_\mathrm{I}^2} \\ &+ \frac{\left(A_\mathrm{V}^2\cos(\varphi_\mathrm{V})\sin(\varphi_\mathrm{V})\right)\times\left(A_\mathrm{I}^2\cos(\varphi_\mathrm{I})\sin(\varphi_\mathrm{I})\right)}{2\,K_\mathrm{V}^2\,K_\mathrm{I}^2}.\end{aligned} \tag{9}$$

The estimated active power standard deviation is given by [12],

$$\sigma_{\hat{\mathrm{P}}} = \sqrt{E\{\hat{P}^2\} - E^2\{\hat{P}\}}\,. \tag{10}$$

Inserting equation (9), and assuming there is no estimation bias ($E\{\hat{P}\} = P$) and making use of (4) leads to

$$\sigma_{\hat{P}} = \frac{1}{\sqrt{2\,M}}\sqrt{V^2\left(\frac{\sigma_\mathrm{I}}{K_\mathrm{I}}\right)^2 + I^2\left(\frac{\sigma_\mathrm{V}}{K_\mathrm{V}}\right)^2 + \frac{4}{M}\left(\frac{\sigma_\mathrm{V}}{K_\mathrm{V}}\right)^2\left(\frac{\sigma_\mathrm{I}}{K_\mathrm{I}}\right)^2}\,. \tag{11}$$

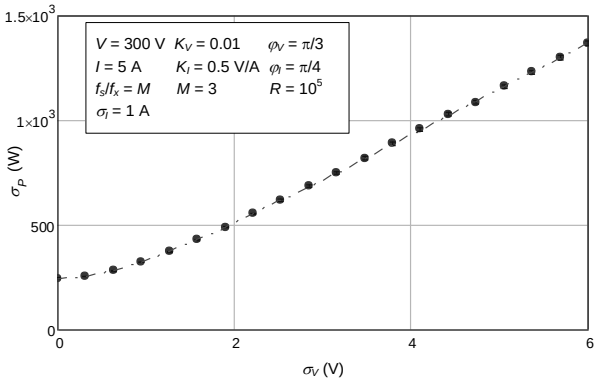

Figure 3. The circles in the graph represent the results of the Monte Carlo study of the standard deviation of the active power estimated using the spectral analysis method, plotted against the standard deviation of the random noise in the ADC voltage measurement channel. The theoretical values given by equation (11) are shown as a dashed line.

This method enables the computation of the standard deviation of active power estimation, considering the real voltage and current values, the quantity of gathered samples, and the standard deviation of the random noise [13] existing at each ADC channel input.

To validate the precision of our calculations, we carried out a Monte Carlo analysis employing simulated ADCs and random noise. This procedure entailed performing active power estimations 10^5 times, each time with different simulated random noise levels, followed by the computation of the standard deviation of the estimated active power. The outcomes of this analysis are illustrated in Figure 3. This figure illustrates the concordance between the simulated and theoretical values.

In Figure 4, you can observe the disparity between these values, with vertical bars denoting the confidence interval for a 99.9% confidence level, derived from the Monte Carlo estimation of the active power estimation standard deviation. Notably, all the vertical bars are centred around zero, signifying that the analytical expression derived aligns consistently with the Monte Carlo simulation results.

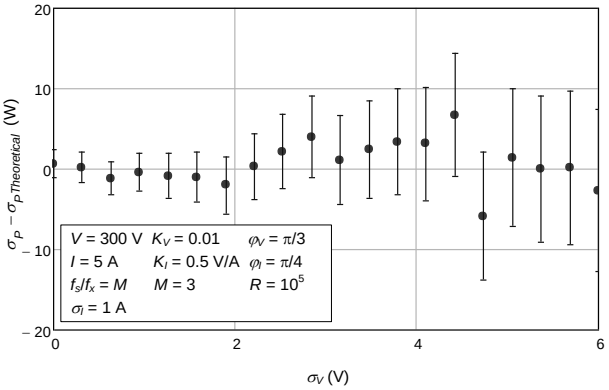

Figure 4. In this graph, we present the contrast between the outcomes of the Monte Carlo analysis and the theoretical values derived from equation (11) for the standard deviation of active power estimation when employing the spectral analysis method. These values are represented as circular data points, plotted against the standard deviation of random noise within the ADC voltage measurement channel. The vertical bars depicted on the graph represent the confidence intervals resulting from the Monte Carlo estimation of the standard deviation of active power estimation. It's noteworthy that all of these vertical bars are centred around zero, affirming the congruity between the analytical expression and the Monte Carlo simulation outcomes.

4. DISCRETE INTEGRATION METHOD

The voltage waveform at each ADC channel input is proportional to the voltage and current signals used to calculate the active power, as expressed by equations (3). The ADC then samples these voltages at a specific sampling rate, f_s, resulting in the sampled voltages being expressed as:

$$\begin{aligned} v_{\mathrm{ADC}_{1}i} &= V\,K_{\mathrm{V}} \cdot \cos(\Omega \cdot i + \varphi_{\mathrm{V}}) + n_{\mathrm{ADC}_{1}i} \\ v_{\mathrm{ADC}_{2}i} &= I\,K_{\mathrm{I}} \cdot \cos(\Omega \cdot i + \varphi_{\mathrm{I}}) + n_{\mathrm{ADC}_{2}i}\,, \end{aligned} \tag{12}$$

where Ω, given by ω/f_{s} represents the digital frequency.

Within the discrete integration method, the voltage waveforms corresponding to voltage and current are multiplicatively combined on a per-sample basis. As depicted in equation (12), this yields:

$$\begin{aligned} v_{\mathrm{ADC}_{1}i} \cdot v_{\mathrm{ADC}_{2}i} &= \frac{1}{2}\,V\,I\,K_{\mathrm{V}}\,K_{\mathrm{I}}\cos(\varphi_{\mathrm{V}} - \varphi_{\mathrm{I}}) \\ &+ \frac{1}{2}\,V\,I\,K_{\mathrm{V}}\,K_{\mathrm{I}}\cos(2\,\Omega\,i + \varphi_{\mathrm{V}} + \varphi_{\mathrm{I}}) \\ &+ n_{\mathrm{ADC}_{1}i} \cdot n_{\mathrm{ADC}_{2}i} + n_{\mathrm{ADC}_{2}i} \cdot V\,K_{\mathrm{V}}\cos(\Omega\,i + \varphi_{\mathrm{V}}) \\ &+ n_{\mathrm{ADC}_{1}i} \cdot I\,K_{\mathrm{I}}\cos(\Omega\,i + \varphi_{\mathrm{I}})\,. \end{aligned} \tag{13}$$

The power estimation involves computing the average of this vector and subsequently dividing it by the factor $K_{\mathrm{V}}\,K_{\mathrm{I}}$

$$\hat{P} = \frac{1}{K_{\mathrm{V}}\,K_{\mathrm{I}}} \cdot \frac{1}{M}\sum_{i=1}^{M} v_{\mathrm{ADC}_{1}i}\,v_{\mathrm{ADC}_{2}i}\,. \tag{14}$$

By inserting equation (13) and taking into account that the data acquisition occurs over an integer number of complete periods, we arrive at:

$$\hat{P} = \frac{1}{K_{\mathrm{V}}\,K_{\mathrm{I}}}\left[\begin{array}{l} \frac{1}{2}\,V\,I\,K_{\mathrm{V}}\,K_{\mathrm{I}}\cos(\varphi_{\mathrm{V}} - \varphi_{\mathrm{I}}) + \\ \quad \frac{1}{M}\sum_{i=1}^{M} n_{\mathrm{ADC}_{1}i} \cdot n_{\mathrm{ADC}_{2}i} + \\ \frac{V\,K_{\mathrm{V}}}{M}\sum_{i=1}^{M} n_{\mathrm{ADC}_{2}i}\cos(\Omega\,i + \varphi_{\mathrm{V}}) + \\ \quad \frac{I\,K_{\mathrm{I}}}{M}\sum_{i=1}^{M} n_{\mathrm{ADC}_{1}i}\cos(\Omega\,i + \varphi_{\mathrm{I}}) \end{array}\right]. \tag{15}$$

The variance of the estimator can be derived from equation (15) by assuming that the additive noise terms are independent of the signals.

$$\begin{aligned} VAR\{\hat{P}\} &= \frac{1}{M^2\,K_{\mathrm{V}}^2\,K_{\mathrm{I}}^2} VAR\left\{\sum_{i=1}^{M} n_{\mathrm{ADC}_{1}i} \cdot n_{\mathrm{ADC}_{2}i}\right\} \\ &+ \frac{V^2}{M^2\,K_{\mathrm{I}}^2} VAR\left\{\sum_{i=1}^{M} n_{\mathrm{ADC}_{2}i}\cos(\Omega\,i + \varphi_{\mathrm{V}})\right\} \\ &+ \frac{I^2}{M^2\,K_{\mathrm{V}}^2} VAR\left\{\sum_{i=1}^{M} n_{\mathrm{ADC}_{1}i}\cos(\Omega\,i + \varphi_{\mathrm{I}})\right\}. \end{aligned} \tag{16}$$

The variance encountered in the first summation in (16) is, by definition,

$$\begin{aligned} &VAR\left\{\sum_{i=1}^{M} n_{\mathrm{ADC}_{1}i} \cdot n_{\mathrm{ADC}_{2}i}\right\} = \\ &E\left\{\left[\sum_{i=1}^{M} n_{\mathrm{ADC}_{1}i} \cdot n_{\mathrm{ADC}_{2}i}\right]^2\right\} - E^2\left\{\sum_{i=1}^{M} n_{\mathrm{ADC}_{1}i} \cdot n_{\mathrm{ADC}_{2}i}\right\}. \end{aligned} \tag{17}$$

This can be written as

$$\begin{aligned} &VAR\left\{\sum_{i=1}^{M} n_{\mathrm{ADC}_{1}i} n_{\mathrm{ADC}_{2}i}\right\} = \\ &\sum_{i,j=1}^{M} E\left\{n_{ADC_{1}i} \cdot n_{ADC_{2}i} \cdot n_{ADC_{1}j} \cdot n_{ADC_{2}j}\right\} \\ &-\left[\sum_{i=1}^{M} E\left\{n_{ADC_{1}i} \cdot n_{ADC_{2}i}\right\}\right]^2. \end{aligned} \tag{18}$$

As the random noises at both ADC inputs are presumed to be independent, the final term in the equation becomes null.

Additionally, the terms of the double summation are non-zero only when $i = j$. We thus have

$$VAR\left\{\sum_{i=1}^{M} n_{\mathrm{ADC}_{1}i} n_{\mathrm{ADC}_{2}i}\right\} = \sum_{i=1}^{M} E\left\{{n_{\mathrm{ADC}_{1}i}}^2\right\} E\left\{{n_{\mathrm{ADC}_{2}i}}^2\right\}. \tag{19}$$

Given that we are dealing with a random noise signal with null mean, its variance is equal to its second moment. The standard deviation of the noise can be different for each channel, represented by σ_{V} and σ_{I}, respectively. Equation (19) then becomes

$$VAR\left\{\sum_{i=1}^{M} n_{\mathrm{ADC}_{1}i} \cdot n_{\mathrm{ADC}_{2}i}\right\} = M\,\sigma_{\mathrm{V}}^2\,\sigma_{\mathrm{I}}^2. \tag{20}$$

Using the variance definition, we can express the other two variance terms in equation (16) which are equivalent but correspond to different variables as follows:

$$\begin{aligned} &VAR\left\{\sum_{i=1}^{M} n_i\cos(\Omega\,i + \varphi)\right\} = \\ &E\left\{\left[\sum_{i=1}^{M} n_i\cos(\Omega\,i + \varphi)\right]^2\right\} \\ &-E^2\left\{\sum_{i=1}^{M} n_i\cos(\Omega\,i + \varphi)\right\}, \end{aligned} \tag{21}$$

where n_i can represent $n_{\mathrm{ADC}_{1}i}$ or $n_{\mathrm{ADC}_{2}i}$.

The expected value of the summation is zero because the noise is considered here a null mean random variable:

$$E\left\{\sum_{i=1}^{M} n_i\cos(\Omega\,i + \varphi)\right\} = \sum_{i=1}^{M} E\{n_i\}\cos(\Omega\,i + \varphi) = 0. \tag{22}$$

The expected value of the square of the sum can be expressed as follows:

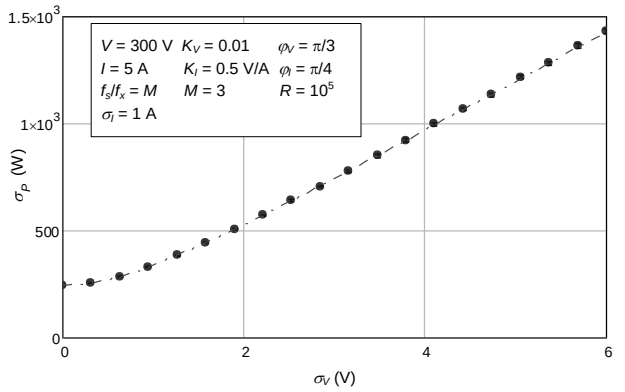

Figure 5. The Monte Carlo analysis outcomes, representing the standard deviation of active power estimated through the discrete integration method in relation to the standard deviation of random noise in the ADC voltage measurement channel (depicted as circles), are juxtaposed with the theoretical values derived from equation (11) (illustrated as a dashed line).

$$E\left\{\left[\sum_{i=1}^{M} n_i \cos(\Omega\, i+\varphi)\right]^2\right\} = \sum_{i,j=1}^{M} E\{n_i\, n_j\} \cos(\Omega\, i+\varphi)\cos(\Omega\, j+\varphi). \quad (23)$$

The only non-zero terms of the double summation are those where $i = j$. We thus have

$$E\left\{\left[\sum_{i=1}^{M} n_i \cos(\Omega\, i+\varphi)\right]^2\right\} = \sum_{i=1}^{M} E\{n_i^2\} \cos^2(\Omega\, i+\varphi), \quad (24)$$

which leads to

$$E\left\{\left[\sum_{i=1}^{M} n_i \cos(\Omega\, i+\varphi)\right]^2\right\} = \frac{M}{2} E\{n_i^2\}. \quad (25)$$

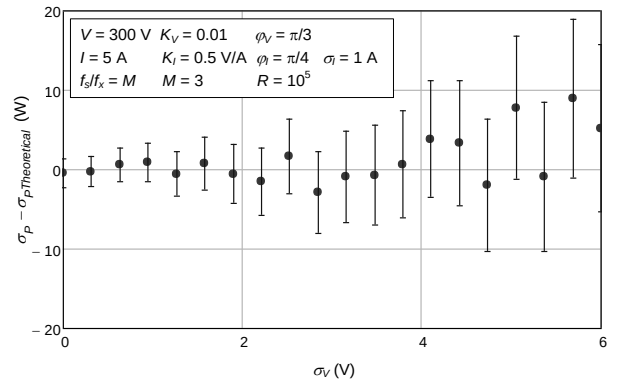

Figure 6. The graph displays the disparity between the Monte Carlo analysis findings for the standard deviation of active power estimation using the discrete integration method and the theoretical values derived from equation (11), with respect to the standard deviation of random noise in the ADC voltage measurement channel. This discrepancy is represented by circular data points. The vertical bars in the figure indicate the confidence intervals for a 99.9% confidence level resulting from the standard deviation estimation.

Considering that the noise has a null mean, the expected value of its square is just its variance. We thus have

$$VAR\left\{\sum_{i=1}^{M} n_i \cos(\Omega\, i+\varphi)\right\} = \frac{M}{2}\,\sigma_n^2\,. \quad (26)$$

Inserting (20) and (26) into (16) leads to

$$VAR\{\hat{P}\} = \frac{1}{2\,M}\left[V^2\left(\frac{\sigma_I}{K_I}\right)^2 + I^2\left(\frac{\sigma_V}{K_V}\right)^2 + 2\left(\frac{\sigma_V}{K_V}\right)^2\left(\frac{\sigma_I}{K_I}\right)^2\right]. \quad (27)$$

The standard deviation of the estimated active power is simply the square root of the variance.

$$\sigma_{\hat{P}} = \frac{1}{\sqrt{2\,M}}\sqrt{V^2\left(\frac{\sigma_I}{K_I}\right)^2 + I^2\left(\frac{\sigma_V}{K_V}\right)^2 + 2\left(\frac{\sigma_V}{K_V}\right)^2\left(\frac{\sigma_I}{K_I}\right)^2}\,. \quad (28)$$

To validate the findings, a Monte Carlo analysis was conducted on the simulated discrete integration method. The results acquired are presented in Figure 5, illustrating a favourable agreement between the simulation and the theoretical values.

The contrast between the results from the Monte Carlo simulation and the theoretical expression (28) is presented in Figure 6, where vertical bars are used to denote confidence intervals at a 99.9% confidence level. Notably, all these bars are centred around zero, affirming the applicability of expression (28) under the specified conditions.

5. ESTIMATOR COMPARISON

Following the derivation of analytical expressions for the standard deviation of active power estimation using both digital techniques, we can now make a comparison. In both methods, the standard deviation of estimation relies on the amplitudes of the voltage and current being measured, as well as the standard deviation of random noise in each ADC channel. It's essential to note that these standard deviations are normalized by the constants K_V and K_I, signifying that what truly matters is the amount of random noise in relation to the input quantities, i.e.,

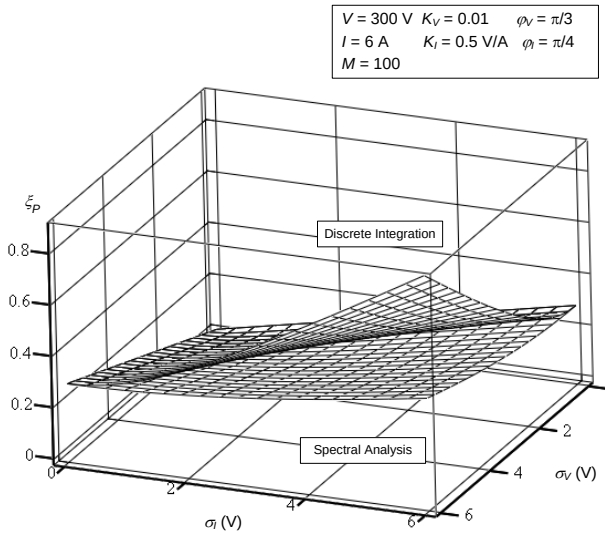

Figure 7. Contrast between the standard deviation of active power estimation employing the spectral analysis method (lower) and the discrete integration method (upper).

voltage and current. Furthermore, in both scenarios, an increase in the number of collected samples leads to a reduction in the standard deviation of the estimated active power.

Upon scrutinizing equations (11) and (28), it becomes evident that the sole distinction lies within the third term enclosed by the square root. The discrete integration method incorporates a factor of 2, while the spectral analysis method integrates a factor of $4/M$. Since M must surpass 2, the $4/M$ factor consistently remains smaller than the 2 factor. Consequently, we can conclude that the spectral analysis method yields a lower standard deviation (enhanced precision) compared to the discrete integration method. Nevertheless, this disparity assumes significance primarily when there is a substantial presence of random noise. In scenarios where such noise is minimal, the third term becomes inconsequential relative to the first two terms beneath the square root, rendering the distinctions between the expressions minimal.

Figure 7 provides a visual representation of this comparison by graphing both analytical expressions against the standard deviation of random noise (in both ADC channels) for a dataset of 100 samples. The displayed surfaces pertain to the normalized active power estimation, as defined by:

$$\xi_{\hat{P}} = \frac{\sigma_{\hat{P}}}{V\,I}. \tag{29}$$

It's noticeable that the two surfaces closely overlap when the random noise is at a low level. Only as the noise level escalates does a disparity between the surfaces become evident. In such instances, the surface associated with the discrete integration method overlays the other, signalling a higher standard deviation in estimation (lower precision).

In this research, we have conducted a comparative analysis of two methods for estimating active power based on digital measurements of voltage and current, focusing on precision in estimation. These two methods are the discrete integration method and the spectral analysis method. We have formulated analytical expressions that facilitate the calculation of the standard deviation of active power estimation, considering the level of random noise and the quantity of acquired samples. These expressions serve to compute confidence intervals for the measurements, constituting a Type B evaluation of uncertainty.

Furthermore, these expressions allow us to ascertain the minimum number of samples necessary to achieve a desired level of precision in the measurement outcomes. While increasing the number of samples enhances precision, it also extends the measurement duration. Determining the minimum requisite number of samples ensures an efficient measurement process in terms of time and memory usage, thereby contributing to cost-effective system implementation.

6. CONCLUSION

The comparison between the two ways of estimating active power from digital measurements of voltage and current has been a subject of extensive analysis, leading to a significant finding that sheds light on their respective strengths and limitations. Specifically, it has been observed that the spectral analysis method outperforms the discrete integration method in terms of precision when subjected to identical measurement conditions. This finding has significant implications for accurate power measurement in various applications.

However, it is important to consider the trade-off associated with the spectral analysis method. While it offers superior precision, it necessitates higher computing power, which relies heavily on the available hardware resources. The computational demands of the spectral analysis method may pose challenges in certain situations, particularly in resource-constrained environments or when dealing with large-scale power monitoring systems. Therefore, the choice between the two methods should take into account the available computational capabilities and the specific requirements of the application.

It is worth noting that the improved precision of the spectral analysis method becomes particularly pronounced in scenarios characterized by the presence of extreme random noise. In such cases, where accurate power measurement is paramount, the spectral analysis method proves to be a more reliable choice. However, in situations with small to moderate levels of noise, both methods exhibit similar levels of precision, making the discrete integration method a viable and computationally efficient alternative.

It is crucial to acknowledge that the analysis presented in this context is limited in scope, as it does not consider certain non-ideal factors that can influence the precision of both methods. Factors such as phase noise, sampling jitter [14], and frequency error can introduce distortions and uncertainties into the measurement process, potentially influencing the performance of each method differently. Furthermore, the nonlinearity inherent in the analog-to-digital converter (ADC) used for digitizing the voltage and current waveforms can introduce errors that need to be accounted for in accurate power estimation.

Given these considerations, further in-depth studies are warranted to explore the impact of these non-ideal factors on the precision and reliability of both methods. It is important to understand how phase noise, sampling jitter, frequency error, and ADC nonlinearity affect the estimation process and to develop appropriate compensation techniques to mitigate their effects [15]-[18]. By addressing these factors, the accuracy and robustness of the active power measurement methods can be enhanced, leading to more reliable and consistent results across a range of measurement scenarios.

Moreover, the analytical expressions derived in this study provide valuable tools for practical implementation. They enable the calculation of confidence intervals for measurements, allowing for the quantification of uncertainties associated with the estimated active power values. Additionally, these expressions can help determine the minimum number of samples required to achieve a desired level of precision, enabling optimized measurement strategies in terms of time and memory requirements, particularly in microcontroller-based systems. By leveraging these analytical tools, researchers and engineers can develop efficient and reliable power measurement systems tailored to their specific needs.

In conclusion, the comparison of active power estimation methods based on digital measurements of voltage and current waveforms has yielded important insights. The spectral analysis method demonstrates superior precision, albeit with higher computational demands, while the discrete integration method offers a computationally efficient alternative with comparable performance under low to moderate noise levels. However, further investigations are needed to explore the impact of non-ideal factors and develop compensation techniques. The analytical expressions derived in this study provide practical utility in terms of calculating confidence intervals and optimizing measurement strategies, facilitating the development of accurate and efficient power measurement systems.

7. APPENDIX

This appendix is devoted to deriving the second moment of the estimated in-phase and in-quadrature amplitudes of a sine wave, as well as their product, obtained using the three-parameter sine-fitting algorithm recommended in [19].

As per [20], the in-phase amplitude is estimated using the following equation with the set of data points y_i, where ω_a represents the frequency of the sine wave being fitted to the data and t_i are the sampling instants:

$$\widehat{A_1} = \frac{2}{M}\sum_{i=1}^{M} y_i \cos(\omega_a t_i)\,. \tag{30}$$

Likewise, the quadrature component is estimated using

$$\widehat{A_2} = \frac{2}{M}\sum_{i=1}^{M} y_i \sin(\omega_a t_i)\,. \tag{31}$$

As per the sine wave model, the data points are obtained by corrupting a sine wave with additive noise (d):

$$y_i = C + A\cos(\omega_x t_i + \varphi) + d_i\,, \tag{32}$$

where the variables C, A, ω_x and φ are the offset, amplitude angular frequency and initial phase of sinusoidal signal that resulted in the data points extracted.

In this context, we assume that the frequency used for fitting the sine wave to the data is known and equal to the frequency of the sine wave we are trying to estimate (i.e., $\omega_x = \omega_a$).

Inserting (32) into (30) leads to

$$\widehat{A_1} = \frac{2}{M}\sum_{i=1}^{M}[C + A\cos(\omega_a t_i + \varphi) + d_i]\cos(\omega_a t_i)\,. \tag{33}$$

The square of the estimated in-phase amplitude is

$$\widehat{A_1}^2 = \frac{4}{M^2}\sum_{i,j=1}^{M}\left\{\begin{matrix}[C + A\cos(\omega_a t_i + \varphi) + d_i]\times\\ [C + A\cos(\omega_a t_j + \varphi) + d_j]\times\\ \cos(\omega_a t_i)\cos(\omega_a t_j)\end{matrix}\right\}. \tag{34}$$

After performing some algebraic manipulation and considering that the data covers a whole number of periods of the sine wave, we obtain:

$$\widehat{A_1}^2 = \frac{4}{M^2}\cdot \sum_{i,j=1}^{M}\left[\frac{1}{4}A^2\cos^2(\varphi) + d_i\, d_j\cos(\omega_a t_i)\cos(\omega_a t_j)\right]. \tag{35}$$

This, in turn, can be written as

$$\widehat{A_1}^2 = A^2\cos^2(\varphi) + \frac{4}{M^2}\sum_{i,j=1}^{M}[d_i\, d_j\cos(\omega_a t_i)\cos(\omega_a t_j)]. \tag{36}$$

The expected value of the square in-phase amplitude estimation is

$$E\left\{\widehat{A_1}^2\right\} = A^2\cos^2(\varphi) + \frac{4}{M^2}\sum_{i,j=1}^{M} E\{d_i\, d_j\}\cos(\omega_a t_i)\cos(\omega_a t_j)\,. \tag{37}$$

The expected value inside the double summation is only non-zero when $i = j$, since d is a random variable with a null mean. We thus have

$$E\left\{\widehat{A_1}^2\right\} = A^2\cos^2(\varphi) + \frac{2}{M}\sigma^2\,, \tag{38}$$

where σ is the random noise standard deviation.

A similar derivation can be applied to the in-quadrature amplitude estimate, which yields

$$E\left\{\widehat{A_2}^2\right\} = A^2\sin^2(\varphi) + \frac{2}{M}\sigma^2. \tag{39}$$

It can also be demonstrated that the expected value of the product between the in-phase and in-quadrature amplitudes is expressed as

$$E\{\widehat{A_1}\,\widehat{A_2}\} = A^2\cos(\varphi)\sin(\varphi). \tag{40}$$

8. REFERENCES

[1] F. Corrêa Alegria, P. Girão, V. Haasz, A. Cruz Serra, Performance of Data Acquisition Systems from the User's Point of View, IEEE Transactions on Instrumentation and Measurement, vol. 53, n 4, August 2004, pp. 907-914. DOI: 10.1109/TIM.2004.830757

[2] F. Corrêa Alegria, P. Girão, V. Haasz, A. Serra, .Performance of Data Acquisition Systems from User's Point of View., IEEE Instrumentation and Measurement Technology Conf., Vail, Colorado, USA, 20-22 May 2003, pp. 940-945. DOI: 10.1109/IMTC.2003.1207891

[3] F. Corrêa Alegria, A. Cruz Serra, Comparison Between Two Digital Methods for Active Power Measurement, IEEE-ICIT 2010 – IEEE Int. Conf. on Industrial Technology, Vina del Mar, Valparaiso, Chile, 14-17 March 2010, pp. 173-178. DOI: 10.1109/ICIT.2010.5472681

[4] Xiaofan Jiang, P. Dutta, D. Culler, I. Stoica, Micro power meter for energy monitoring of wireless sensor networks at scale, Proc. of the 6th Int. Conf. on Information Processing in Sensor Networks, Cambridge, Massachusetts, USA, 25 - 27 April 2007, pp. 186-195. DOI: 10.1109/IPSN.2007.4379678

[5] H. Serra, J. Correia, A. J. Gano, A. M. de Campos, I. Teixeira, Domestic Power Consumption Measurement and Automatic Home Appliance Detection, IEEE Int. Workshop on Intelligent Signal Processing, Faro, Portugal, 1-3 September 2005, pp. 128-132. DOI: 10.1109/WISP.2005.1531645

[6] A. Carullo, M. Parvis, A. Vallan, Low-cost power meter for the characterisation of inverter-fed electrical machines, IEEE Instrumentation and Measurement Technology Conf., Ottawa, Canada, 19-21 May 1997, pp. 270-275. DOI: 10.1109/IMTC.1997.603955

[7] Ch.-P. Young, M. J. Devaney, Digital Power Metering Manifold, IEEE Instrumentation and Measurement Technology Conf., Ottawa, Canada, 19-21 May 1997, pp. 1403-1406. DOI: 10.1109/IMTC.1997.612430

[8] S. Svensson, Power measurement techniques for non-sinusoidal conditions, Ph.D. thesis, 1999.

[9] IEEE Standard 1159-1995, IEEE Recommended Practice for Monitoring Electric Power Quality, IEEE, 1995. DOI: 10.1109/IEEESTD.1995.79050

[10] F. Corrêa Alegria, A. Cruz Serra, Gaussian jitter-induced bias of sine wave amplitude estimation using three-parameter sine fitting, IEEE Transactions on Instrumentation and Measurement, vol. 59, no. 9, September 2010, pp. 2328-2333.
DOI: 10.1109/TIM.2009.2034576

[11] F. Corrêa Alegria, A. Cruz Serra, Uncertainty of the estimates of sine wave fitting of digital data in the presence of additive noise, Proc. of the 2006 IEEE Instrumentation and Measurement Technology Conf., Sorrento, Italy, 24-27 April 2006.
DOI: 10.1109/IMTC.2006.328187

[12] A. Papoulis, Probability, Random Variables and Stochastic Processes, McGraw-Hill, 3rd edition, 1991.
DOI: 10.2307/1266379

[13] F. Corrêa Alegria, A. Cruz Serra, Uncertainty of ADC random noise estimates obtained with the IEEE 1057 standard test, IEEE Transactions in Instrumentation and Measurement, vol. 54, 2005, no. 1, pp. 110-116.
DOI: 10.1109/TIM.2004.840226

[14] S. Shariat-Panahi, F. Corrêa Alegria, A. Mànuel, A. Cruz Serra, IEEE 1057 jitter test of waveform recorders, IEEE Transactions on Instrumentation and Measurement 58 (7), 2009, pp. 2234-2244.
DOI: 10.1109/TIM.2009.2013674

[15] A. Cruz Serra, F. Corrêa Alegria, L. Michaeli, P. Michalko, J. Saliga, Fast ADC testing by repetitive histogram analysis, 2006 IEEE Instrumentation and Measurement Technology Conf., Sorrento, Italy, 24-27 April 2006.
DOI: 10.1109/IMTC.2006.328161

[16] F. Corrêa Alegria, A. Moschitta, P. Carbone, A. Cruz Serra, D. Petri, Effective ADC linearity testing using sinewaves, IEEE Transactions on Circuits and Systems I: Regular Papers 52 (7) , 2005, pp. 1267-1275.
DOI: 10.1109/TCSI.2005.851393

[17] F. Corrêa Alegria, A. Cruz Serra, Influence of Frequency Errors in the Variance of the Cumulative Histogram, IEEE Transactions on Instrumentation and Measurement, vol. 50, n 2, April 2001, pp. 461-464.
DOI: 10.1109/19.918166

[18] F. Corrêa Alegria, A. Cruz Serra, Uncertainty in the ADC transition voltages determined with the histogram method, Proc. of the 6th Workshop on ADC Modeling and Testing, Lisbon, 13-14 September 2001. Online [Accessed 19 December 2023] https://www.imeko.org/publications/tc4-2001/IMEKO-TC4-2001-091.pdf

[19] IEEE Standard for Digitizing Waveform Recorders, IEEE Std. 1057-2007, April 2008.
DOI: 10.1109/IEEESTD.2008.8291822

[20] F. Corrêa Alegria, Bias of amplitude estimation using three-parameter sine fitting in the presence of additive noise, Measurement, vol. 42, 2009, pp. 748–756.
DOI: 10.1016/j.measurement.2008.12.006